CORA Cork Open Research Archive
Cartlann Taighde Oscailte Chorcaí

Title	Virtual synchronous-machine control of voltage-source converters in a low-voltage microgrid
Author(s)	Hogan, Diarmaid J.; Gonzalez-Espin, F.; Hayes, John G.; Lightbody, Gordon; Albiol-Tendillo, L.; Foley, Ray
Publication date	2016-10-27
Original citation	Hogan, D. J., Gonzalez-Espin, F., Hayes, J. G., Lightbody, G., Albiol-Tendillo, L. and Foley, R. (2016) 'Virtual synchronous-machine control of voltage-source converters in a low-voltage microgrid', 18th European Conference on Power Electronics and Applications (EPE'16 ECCE Europe), Karlsruhe, Germany, 5-9 September. Institute of Electrical and Electronics Engineers (IEEE), pp. 1-10. doi:10.1109/EPE.2016.7695503
Type of publication	Conference item
Link to publisher's version	http://ieeexplore.ieee.org/xpl/mostRecentIssue.jsp?punumber=7588973 http://dx.doi.org/10.1109/EPE.2016.7695503 Access to the full text of the published version may require a subscription.
Rights	© 2016, IEEE. Personal use of this material is permitted. Permission from IEEE must be obtained for all other uses, in any current or future media, including reprinting/republishing this material for advertising or promotional purposes, creating new collective works, for resale or redistribution to servers or lists, or reuse of any copyrighted component of this work in other works.
Item downloaded from	http://hdl.handle.net/10468/3534

UCC

University College Cork, Ireland
Coláiste na hOllscoile Corcaigh

Virtual Synchronous-Machine Control of Voltage-Source Converters in a Low-Voltage Microgrid

D. J. Hogan[1], F. Gonzalez-Espin[3], J. G. Hayes[1], G. Lightbody[1,2], L. Albiol-Tendillo[3], R. Foley[3]
[1]Power Electronics Research Laboratory, University College Cork, Cork City, Ireland
[2]MaREI-SFI Research Centre, University College Cork, Cork City, Ireland
[3]UTRC-Ireland, Penrose Warf Business Centre, Cork City, Ireland
E-Mail: diarmaid.hogan@umail.ucc.ie
URL: http://www.perl.ucc.ie, http://www.utrc.utc.com

Acknowledgements

Keywords

Virtual Synchronous-Machine, Voltage-Source Converter, Vector Control, Microgrid, Ancillary Services

Abstract

In order to facilitate the further integration of distributed renewable generation into existing power systems, enhanced control schemes for grid-tied power electronic converters are necessary to ensure non-synchronous power sources can provide power and support to the grid. The virtual-synchronous-machine concept proposes the use of control schemes to enable static generators to operate with the dynamics of rotating synchronous generators. In this paper, a control scheme is presented based on the principle of active-power synchronization to regulate the active power of a grid-tied voltage-source converter based on an emulation of the synchronous-machine swing equation. Design of a cascaded inner-loop voltage and resonant current control is presented to regulate the output voltage as specified via the outer-loop virtual-machine control scheme responsible for power regulation. The performance of this control scheme is investigated within the context of microgrid operation for the provision of active and reactive power to the system, and microgrid frequency support. Experimental validation is provided via the use of a 15 kVA three-phase VSC in a 90 kVA 400V microgrid.

1. Introduction

Due to the increasing penetration of renewable generation on the grid and a shift from centralized to distributed generation, the electrical grid is facing a number of significant challenges as the system transitions toward a smart grid. The use of microgrids is seen as being a potential fundamental component of future electrical networks, enabling district, campus and building level systems for example to optimize generation and load demand while providing enhanced security of supply and power quality. The role of power electronics as part of generation (specifically three-phase voltage-source converters (VSCs) as considered here), energy storage and controllable loads are seen as being vital components in the facilitation of the smart grid and future electrical network [1].

The operation of industrial microgrids is underpinned by the use of synchronous generation. Additional VSC interfaced generation, operating as controlled current sources, can be used to offset load demand, reduce energy costs, improve environmental impact, etc. [2]. Indeed this is analogous to the operation of the wider utility-grid. However, as an increasing percentage of the available system generation is being provided by non-synchronous generators, the resulting loss of inertia in the system can lead to degraded performance, including grid-frequency instability [3]. Conventional grid-tied VSC control schemes rely on vector current controls to regulate output power to the grid. These controls generally provide excellent regulation of output current, but their dynamics are fundamentally

different than the synchronous grid to which they are connected [4]. The increasing proportion of non-synchronous generation on the grid will lead to a loss of inertia, potentially resulting in degraded power system performance. There is, therefore, a push towards the development of VSC control schemes which can cooperate in a more seamless way than existing systems while also being capable of providing ancillary services for grid support, in a similar way as provided by existing synchronous generators [5].

The concept of controlling grid-tied VSCs to emulate the dynamics of synchronous generators has become an active area of research in recent years. In [6], a VSM emulation scheme uses the stationary reference-frame (StRF) dynamic equations of the SG to regulate output active and reactive power via direct PWM setpoint specification. A model-based control design approach is used in [4], [7] to develop a control loop to regulate output power and support grid voltage for HVDC applications. However this analysis is not supported by experimental validation. Some VSM methods rely on the use of additional control loops such as phase-locked loops (PLL) to provide estimation of grid parameters or synchronization [8]. Other machine emulation strategies have also been developed, such as a virtual induction-generator as proposed in [9]

System operators will look towards the evolving grid codes to determine areas whereby it is possible to develop and provide additional value-added services to their system. The capability of virtual-machine-enabled VSCs to participate in the provision of ancillary services is a significant motivation for the research and development of VSM control schemes. Virtual inertia will allow for the utilization of non-synchronous generators to participate in grid-frequency support, while reactive power regulation will enable bus voltage regulation and fault ride-through capabilities [10].

This paper proposes a VSM control scheme utilizing an inner-outer loop VSC control scheme to facilitate regulation of the output voltage of the LCL filter and emulation of the output power dynamics of a synchronous generator. The inner-loop consists of a cascaded voltage-current control loop implemented in the synchronous reference-frame (SRF) to regulate output capacitor voltage. Resonant VPI current controls are included to improve output current THDi and improve disturbance rejection. The outer VSM control loop enables control of the active power using a lead-lag control transfer function to emulate the dynamics of a synchronous generator, while reactive power is regulated using an adapted low-pass filtered PI controller. Validation of the proposed control scheme is carried out in a low-voltage microgrid laboratory whereby a 15 kVA three-phase VSC is configured as the VSM operating in parallel with a 90 kVA grid emulator.

This paper is organized as follows: The principle of operation and proposed control scheme is discussed in Section 2. The design of the inner-loop controls is detailed in Section 3, with the development of the VSM outer control loop presented in Section 4. Experimental analysis and discussion are included in Section 5.

2. Operation of Virtual Synchronous Machine

A. Principle of Operation

The grid-tied VSC can be represented as a synchronous voltage source connected to the grid/microgrid bus via an impedance, comprised of the equivalent VSC output impedance (L_t, r_t), and the grid impedance (L_g, r_g), as illustrated in Fig. 1.
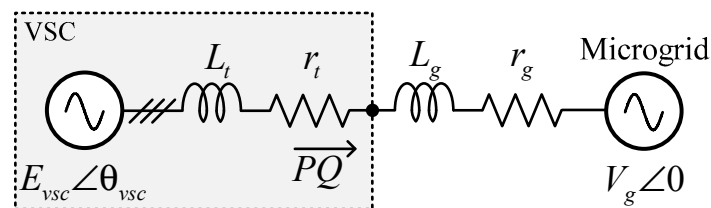

Fig. 1. Equivalent circuit of a three-phase grid-tied VSC

Correspondingly, the active and reactive power injected to the grid by the VSC is given by:

$$P = \frac{3}{Z_{eq}}\left[\left(E_{vsc}V_g\cos\theta_{vsc} - V_g^2\right)\cos\phi_{eq} + E_{vsc}V_g\sin\theta_{vsc}\sin\phi_{eq}\right] \tag{1}$$

$$Q = \frac{3}{Z_{eq}}\left[\left(E_{vsc}V_g\cos\theta_{vsc} - V_g^2\right)\sin\phi_{eq} + E_{vsc}V_g\sin\theta_{vsc}\cos\phi_{eq}\right] \tag{2}$$

where E_{vsc} and θ_{vsc} are the voltage magnitude and phase of the VSC, V_g is the voltage at the point of common coupling to the microgrid, and $Z_{eq}\angle\phi_{eq}$ is the equivalent output impedance accounting for the output filter and grid impedance (if it is known). Assuming that the system is predominantly inductive, meaning relative decoupling of the active and reactive powers as can be considered to be the case in higher power systems, the resulting expressions for P and Q are given as:

$$P = 3\frac{E_{vsc}V_g}{X_{eq}}\sin\theta_{vsc}, \tag{3}$$

$$Q = 3\frac{E_{vsc}V_g\cos\theta_{vsc} - V_g^2}{X_{eq}}. \tag{4}$$

This analysis underpins the operating principle of synchronous generators whereby active output power is regulated via control of the voltage phase difference between the SG and the PCC, while reactive power can be regulated by controlling the voltage magnitude difference. The principle of operation for the VSM utilizes a control strategy to emulate the electromechanical dynamics of a SG to regulate the active and reactive power flow of the VSC. The dynamics of a SG are governed by the swing equation, which is given by;

$$\frac{d\omega_{sg}}{dt} \approx \frac{1}{2H}\left(P^* - P - D\left(\omega_{sg} - \omega_g\right)\right) \tag{5}$$

where ω_{sg} is the angular frequency of the SG, ω_g is the angular frequency of the grid, P is the output power, P^* is the input (setpoint) power, D is a damping coefficient, and H is the constant of inertia.

B. Proposed Control Scheme

The proposed control scheme for the grid-tied VSC is illustrated in Fig. 2. This control scheme utilizes a power-synchronization controller to regulate output active power, via control of the phase angle of the output capacitor voltage, e_c. Use of a lead-lag control transfer function referred to as inertial-droop control is capable of emulating the dynamics of the synchronous-generator swing equation. PI control is implemented to regulate the output reactive power through adjustment of the output voltage magnitude. This VSM control loop generates the voltage and phase references for the inner cascaded voltage-current control loop, responsible for regulating the output voltage on the capacitor of the LCL filter interfacing the VSC to the microgrid. To facilitate start-up, a soft-start synchronization control scheme is implemented to satisfy synchronization criteria before connection to the grid.
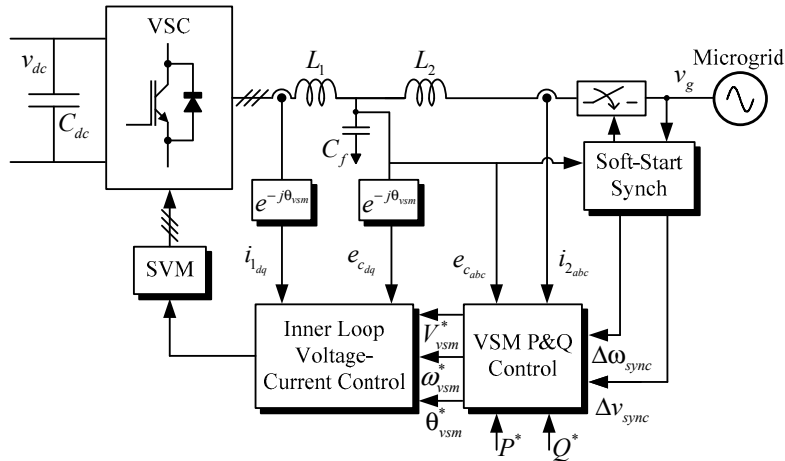

Fig. 2. Proposed VSM control scheme for the grid-tied VSC

3. Inner-Loop Control of LCL Filter Output Voltage

To facilitate regulation of the output voltage on the LCL filter capacitor, a cascaded voltage-current control scheme is implemented in the SRF as illustrated in Fig. 3. This control scheme enables fast and bounded control of the output current and voltage, with PI controls being capable of providing excellent regulation of system states in the SRF along with resonant current controllers being used in parallel to enhance output current harmonic rejection and improve output THDi [11]. An additional virtual-impedance loop allows for adjustment of the output impedance of the VSC as seen by the grid to provide enhanced decoupling of the active and reactive power regulation and improved damping [12]. The voltage magnitude reference generated via the reactive power controller, discussed in Section 4.B, is passed through this virtual impedance resulting in the capacitor voltage reference as given by (6) and (7), where r_v and L_v are the virtual resistance and inductance variables;

$$e_{c_d}^* = V_{vsm}^* - i_{1_d} r_v + i_{1_q} \omega_{vsm} L_v, \tag{6}$$

$$e_{c_q}^* = -i_{1_q} r_v - i_{1_d} \omega_{vsm} L_v. \tag{7}$$

Design of the primary control loops is facilitated via the SRF small-signal model of the three-phase VSC, as given by [13], to obtain the transfer functions relating the output current to the duty cycle and the output current to the capacitor voltage as seen in (9) and (11).
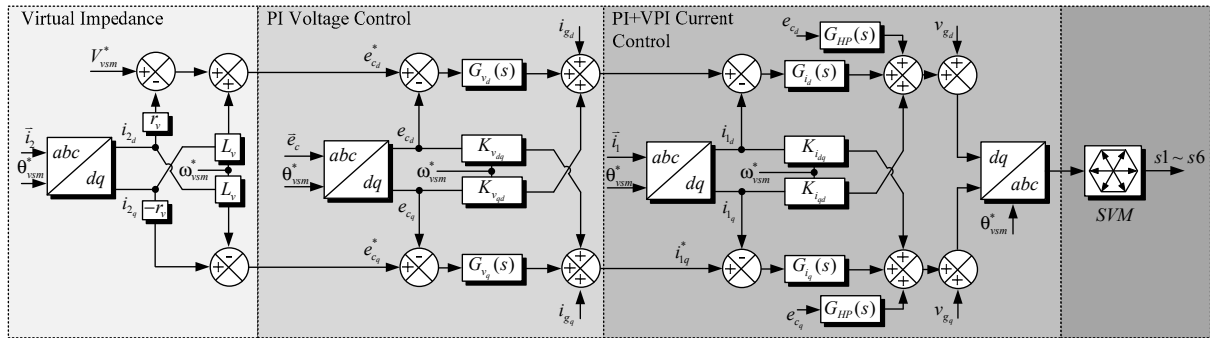

Fig. 3. Cascaded voltage-current control scheme including virtual-impedance implemented in the SRF

A. PI+VPI Resonant Current-Control

This innermost control-loop of the primary-control scheme is tasked with the regulation of the current through the inverter-side inductor, L_1. The design of the current-control scheme typically utilizes additional control elements to mitigate undesired system effects and disturbances. It is also necessary to consider decoupling of the d and q axis, mitigation of harmonic disturbances from the system (using resonant controls in this case), and damping of the LCL filter resonance as illustrated in Fig. 3. LCL active damping is facilitated here using a high-pass feedback measure of the capacitor voltage to emulate derivative feedback [14].

The use of resonant-current controls has been widely discussed in relation to their implementation as part of enhanced current-controlled voltage-source converters providing improved output THDi for grid-tied applications [15]. These resonant controls have been shown to provide improved performance in harmonic current rejection compared with proportional-resonant (PR) controls and show enhanced stability when compensating for higher frequency harmonics due to improved phase response. In this application, VPI controls are implemented in parallel with the PI controllers to provide regulation of the fundamental along with the 2nd, 6th and 12th harmonics in the SRF. The resulting transfer function for this PI+VPI controller is given by:

$$Gi_d(s) = \frac{ki_p s + ki_i}{s} + \sum_{h \in H} 2 \frac{k_p^h s^2 + k_r^h}{s^2 + (h\omega_{vsm})^2}, \tag{8}$$

where ki_p and ki_i are the PI control gains, k_p^h and k_r^h are the proportional and resonant gains of the VPI controller, where $H=\{2,6,12\}$. The small-signal d-axis current-control loop is illustrated in Fig. 4 (a), along with the resulting open loop transfer function given by:

$$T_{i_d}(s) = Gi_d(s) \cdot G_{PWM}(s) \cdot \frac{\tilde{i}_{1d}(s)}{\tilde{d}_d(s)}, \tag{9}$$

where $G_{PWM}(s)$ is a second order Padé approximation of the PWM delay. Design of the q-axis current controls can be considered equivalent due to decoupling of the paths and symmetry of the axes. Bode plot analysis is used to investigate selection of the gains for the current controls. Design of the VPI gains is facilitated through pole placement, with the controller zeroes being placed such that they cancel the plant pole resulting from the output filter inductors, $k_r^h = k_p^h \left((r_1 + r_2)/(L_1 + L_2) \right)$. Selection of the PI gains are used to determine the phase margin and bandwidth of the loop, with the resulting open-loop Bode plot given by Fig. 5 (a), where the resulting open-loop bandwidth is 460 Hz with a phase margin of 75°.

B. PI Voltage-Control

Output capacitor voltage, e_c, is regulated using PI control:

$$Ge_d(s) = \frac{ke_p s + ke_i}{s}, \tag{10}$$

where ke_p and ke_i are the PI voltage control gains. The output of this controller specifies the i_1 current reference for the current-control loop.

The design of the capacitor voltage control loop is predicated on the appropriate design of the inner current loop as detailed previously. The small-signal d-axis voltage control loop is illustrated in Fig. 4 (b), the open-loop transfer function, including the closed-loop transfer function of the current-loop, is given as:

$$T_{e_{cd}}(s) = Ge_d(s) \cdot \frac{T_{i_d}(s)}{1 + T_{i_d}(s)} \cdot \frac{\tilde{e}_{cd}(s)}{\tilde{i}_{1d}(s)}. \tag{11}$$
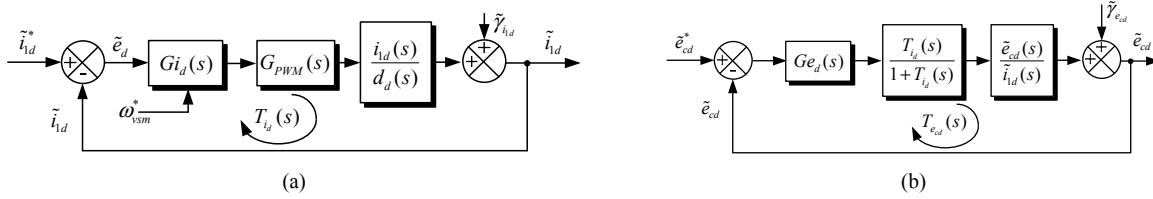

Fig. 4. (a) Small-signal d-axis current control loop (b) Small-signal d-axis voltage control loop

Design of the voltage PI control gains is again facilitated through analysis of the Bode plot of the open-loop system illustrated in Fig. 5 (b). It is important to design the outer voltage-loop bandwidth to be significantly slower than the current loop to minimize interaction. In this situation the resulting open-loop bandwidth is 2 Hz with a phase margin of 92°. Loop bandwidth is limited as a result of the small gain margin (~10dB), however this is not a vital issue since voltage regulation is mainly concerned with disturbance rejection.
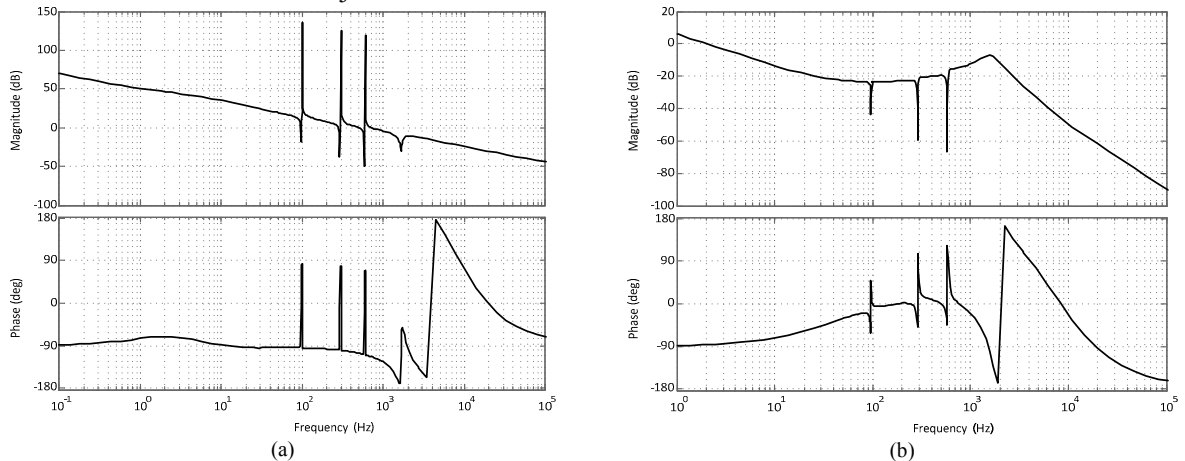

Fig. 5. Open-loop Bode plots for (a) d-axis current loop, T_{id} (b) d-axis voltage loop, T_{ecd}

4. Virtual-Synchronous-Machine Output Power Regulation Scheme

The outer control structure for the grid-tied VSC is illustrated in Fig. 6 (a), where a measurement of the instantaneous output power, P and Q, is calculated via measurement of the capacitor voltage and output current. The active and reactive power controllers are designated as $G_P(s)$ and $G_Q(s)$ and the nominal output voltage frequency and magnitude setpoints are specified by ω^* and v^*. This control scheme then generates the voltage magnitude reference, V_{vsm}^*, for the inner control loops discussed in Section 3, and the phase reference, θ_{vsm}^*, for the control reference-frame transformations, which as presented by (12) and (13), will allow for regulation of the power output.

Control over initial synchronization of the converters is vital to ensure safe soft-start when initializing the converter before connecting to the grid, or to re-synchronize an islanded element of the microgrid to the wider grid. VSM control schemes differ significantly from vector controls due to the lack of a direct synchronization control scheme such as the PLL. A proposed synchronization control scheme is illustrated in Fig. 6 (b). The objective of this control element is to satisfy the synchronization criteria by controlling the frequency, phase and amplitude of the voltage across the filter capacitor to minimize discrepancy with V_g, the grid voltage at the point of common coupling [16]. Once these criteria have been satisfied, it is then possible to safely close the breaker, and start operation.
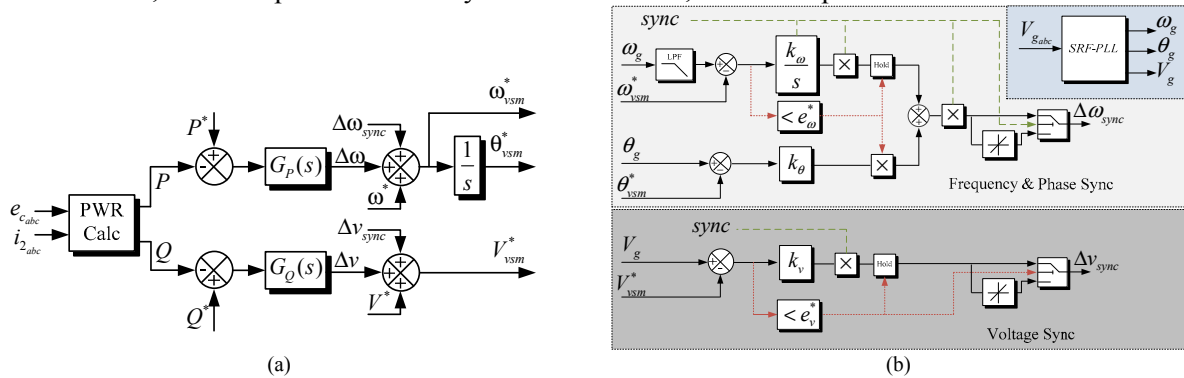

Fig. 6. (a) Active and reactive power VSM control structure (b) Initial soft-start synchronization control scheme

The controller initially synchronizes the frequency via an integral controller, where k_ω is the integral gain, this value is held once the error is reduced below a specified error threshold, e_ω^*, and then synchronizes the phase using proportional control, k_θ. Minimization of the voltage error below the voltage error threshold, e_v^*, is also regulated via a proportional controller, k_v. Once the synchronization criteria are satisfied, the sync signal closes the breaker between the VSC and the grid, and the resulting synchronization signals $\Delta\omega_{sync}$ and Δv_{sync} are reset to zero and the system can begin operation.

A. Inertial-Droop Active-Power Control

Active power is regulated via power-synchronization control of the phase angle difference between the voltage on the LCL filter capacitor and the PCC voltage. Implementation of the swing equation, (5), as part of the control scheme ($G_P(s)$ in Fig. 6 (a)) can enable the VSC to emulate the inertial characteristics of a synchronous generator. A lead-lag active-power synchronization controller, as proposed in [17], [18], is given by (12):

$$G_P(s) = -\frac{m_p s + m_D}{\tau_J s + 1} \tag{12}$$

where τ_J is representative of the equivalent virtual inertia, m_D is the droop gain and m_p is the equivalent damping. Design of these gains will be discussed in relation to the stability analysis of the system.

B. Reactive-Power Regulation

The regulation of the output reactive power of the VSM is facilitated through control over the magnitude of the voltage difference between the LCL capacitor voltage and PCC voltage. For this

application, it was desired to control this output directly, hence a PI controller is used along with a low-pass filter as given by:

$$G_Q(s) = -\frac{n_p s + n_D}{\tau_Q s^2 + s} \tag{13}$$

where n_p and n_D are the PI filter gain, with the capability of designing n_D to allow for a specified system droop. The time constant τ_Q facilitates an averaged measure of the output reactive power and improves system response.

C. Stability Analysis

Through small-signal linearization of the output power equations given by (3) and (4), and assuming ideal performance of the primary control loop, it is possible to obtain the small-signal equations for the output voltage phase and magnitude based on the use of the inertial-droop active power synchronization controller and the PI reactive power regulator as illustrated by the control configuration in Fig. 6 (a):

$$\tilde{\phi}_{cf}(s) = -\frac{m_p s + m_D}{\tau_J s^2 + s}\left[\frac{3V_g \sin\Phi_{cf}\,\tilde{e}_{cf}(s) + 3V_g E_{cf}\cos\Phi_{cf}\,\tilde{\phi}_{cf}(s)}{X_{eq}}\right] \tag{14}$$

$$\tilde{e}_{cf}(s) = -\frac{n_p s + n_D}{\tau_Q s^2 + s}\left[\frac{3V_g \cos\Phi_{cf}\,\tilde{e}_{cf}(s) - 3V_g E_{cf}\sin\Phi_{cf}\,\tilde{\phi}_{cf}(s)}{X_{eq}}\right] \tag{15}$$

Rearranging, and substituting (15) into (14) yields the following fourth-order closed-loop characteristic equation:

$$a_4 s^4 + a_3 s^3 + a_2 s^2 + a_1 s + a_0 = 0 \tag{16}$$

Steady-state values for the output voltage magnitude and phase can be calculated from (1) and (2):

$$\Phi_{cf} = \tan^{-1}\left(\frac{P^* \sin\theta_{eq} - Q^* \cos\theta_g}{P^* \cos\theta_{eq} + Q^* \sin\theta_{eq} + \left(3V_g^2/X_{eq}\right)}\right) \tag{17}$$

$$E_{cf} = \frac{3V_g^2 \cos\theta_{eq} + P^* X_{eq}}{3V_g(\cos\theta_{eq}\cos\Phi_{cf} + \sin\theta_{eq}\sin\Phi_{cf})} \tag{18}$$

Based on this analysis it is possible to investigate the effects of the VSM control gains on the stability and dynamics of the grid-tied VSC. Examination of the root-locus plots illustrated in Fig. 7 shows that as effective virtual inertia in increased, closed-loop poles move closer to the imaginary axis, resulting in a slower system response that eventually becomes oscillatory and unstable. Increasing the droop gain, m_D, results in a faster system response, as closed-loop poles move away from the imaginary axis. Trading off between the desired droop characteristics, system damping and speed of response is vital to obtain a viable virtual machine control scheme.
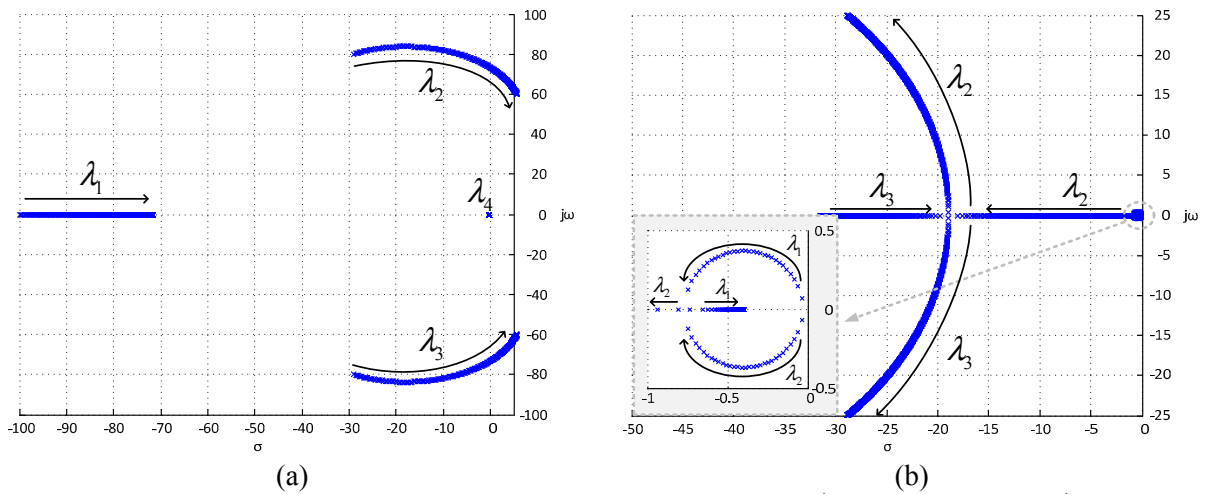

Fig. 7. Root-locus plot of closed loop system poles for (a) $31.8\times10^{-4} < \tau_J < 31.8$ (b) $1\times10^{-4} < m_D < 0.3$

5. Experimental Results

Experimental testing and validation of the proposed VSM control scheme is carried out in a low-voltage three-phase 90 kVA laboratory microgrid as illustrated in Fig. 8. This system is comprised of three grid-tied rapid-prototyping VSCs, one 15 kVA configured as dc-ac interfacing a 5 kWhr Li-ion BESS to the grid, another 15 kVA configured as back-to-back ac-ac and a 90 kVA ac-ac grid emulator. Additional generation equipment includes a 30 kVA three-phase synchronous diesel generator and a 22 kVA wind-turbine emulator. Up to 50 kVA of passive loads are also incorporated as part of the system, including a fault emulator. Supervisory control and interlocking is provided via a Mitsubishi PLC, along with a National Instruments cRIO for data acquisition [19].
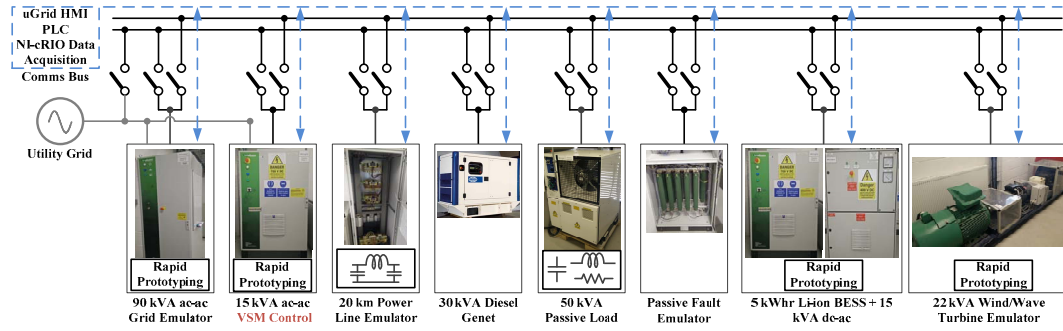

Fig. 8. Microgrid laboratory configuration

For the following experiments, the 90 kVA grid emulator is configured to replicate the dynamics of the synchronous grid, whereby load fluctuations will result in frequency and voltage transients on the microgrid bus [20]. The 15 kVA ac-ac Triphase VSC is configured with the proposed VSM control scheme presented in this paper. System and control parameters are listed in Table I.

Table I: Experimental test parameters and VSM control gains

Parameter	Value	Parameter	Value	Parameter	Value	Parameter	Value
L_1	2.3 mH	r_v	20 mΩ	ke_p	5.7×10^{-3}	m_p	4.5×10^{-5}
L_2	0.93 Mh	ki_p	3.86	ke_i	35.71	m_D	10×10^{-3}
r_1,r_2	0.2 Ω	ki_i	336	k_ω	0.01	τ_J,τ_Q	31.8×10^{-3}
C_f	10 μF	k^h_p	0.6	k_θ	30	n_p	9×10^{-3}
L_v	10 mH	k^h_r	52.3	k_v	2	n_D	1

A. Initial Synchronization and Power Regulation

A demonstration of the frequency and phase synchronization of the system is illustrated in Fig. 9 (a) and (b), where the controller initially brings the frequency below the frequency error threshold specified as $e_\omega^* = 1\times10^{-4}$. The control scheme holds this frequency offset and synchronizes the phase via the proportional controller. The sync signal is triggered and the breaker between the VSC and the microgrid is closed and the converter can begin operation. A comparison of the output current THDi is presented in Fig. 9 (c) and (d), where it can be seen that there is a significant improvement by reducing THDi from 10.61% to 1.92% with the use of the resonant current control scheme. The use of these resonant controls ensures that the output power from the VSM to the local grid does not distort the power quality at the PCC and is capable of complying with grid codes.

The capabilities of the proposed control scheme to regulate are illustrated in Fig. 9 (e) and (f). A 4 kW output power step is demonstrated in Fig. 9 (e), where a fast rise time with a damped response is observed. In Fig. 9 (f) a much slower response is observed for the regulation of the reactive power. Since focus of this paper was mainly aimed at active-power regulation and subsequent grid frequency support, design of the reactive-power control gains was intentionally chosen to provide a slower response, resulting in an approx. 10s settling time. In future testing this design will be evaluated to assess the capabilities for the provision of microgrid bus-voltage support and fault ride-through using reactive power injection.
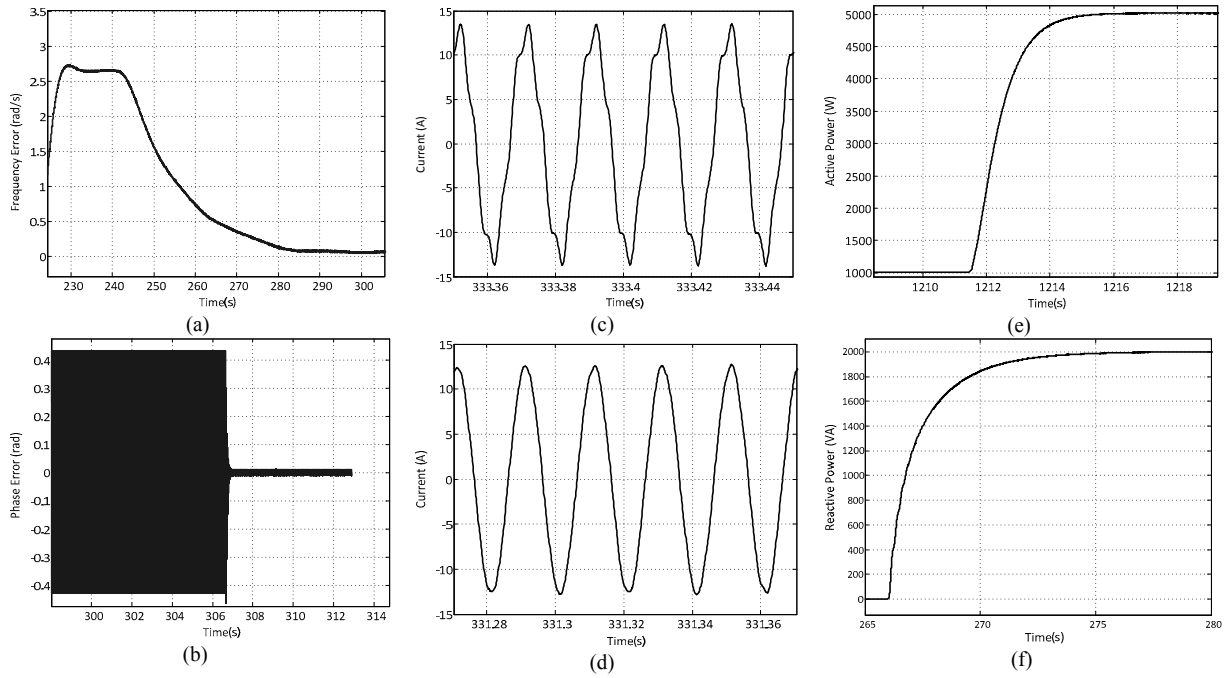
Fig. 9. (a) Soft-start frequency synchronization (b) Soft-start phase synchronization (c) Output current using PI current-control, THDi = 10.61% (d) Output current using PI+VPI current-control, THDi = 1.92% (e) 4 kW step in active output power (f) 2 kVA step in output reactive power

B. Grid Frequency Support

The capability of providing grid frequency support is illustrated in Fig. 10, where load transient of 6 kW is applied to the grid emulator, resulting in a grid frequency transient of -0.046 Hz. The same load transient is applied with the VSM controlled VSC connected in parallel with the grid emulator for three different values of m_D. The resulting improvement of the frequency nadir can be observed, as the droop gain decreases the resulting compensation power injected increases, thus mitigating the resulting transient in the grid frequency. However, the smaller droop gain results in a longer settling time for the output power to return to its steady-state setpoint.
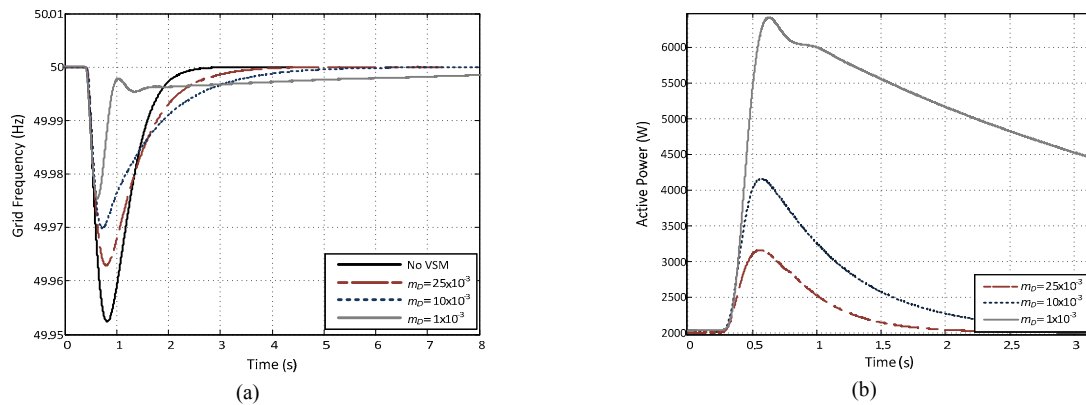

Fig. 10. (a) Frequency support provided by VSC (b) VSC output power during frequency transient

6. Conclusion

The proposed grid-tied VSC control scheme based on the principles of emulating the dynamic characteristics of a synchronous generator has been designed and validated in a laboratory microgrid. This control scheme has been shown to be capable of maintaining synchronism with the grid through active-power synchronization, a distinct difference in operating principle compared with PLL synchronized vector control schemes. Experimental results demonstrate the enhanced output THDi resulting from use of VPI resonant current-controls to mitigate disturbances. Accurate and fast

regulation of the output power is demonstrated, along with the capability to provide frequency support to the microgrid through active-power injection during frequency transients.

References

[1]   D. Manz, R. Walling, N. Miller, B. LaRose, R. D'Aquila, and B. Daryanian, "The Grid of the Future: Ten Trends That Will Shape the Grid Over the Next Decade," *IEEE Power Energy Mag.*, vol. 12, no. 3, pp. 26–36, May 2014.

[2]   S. Masiello, R.; Venkata, "Microgrids: There May Be One in Your Future [Guest Editorial]," *IEEE Power Energy Mag.*, vol. 11, no. 4, p. 14,93, 2013.

[3]   S. Eftekharnejad, V. Vittal, G. T. Heydt, B. Keel, and J. Loehr, "Impact of Increased Penetration of Photovoltaic Generation on Power Systems," *Power Syst. IEEE Trans.*, vol. 28, no. 2, pp. 893–901, 2013.

[4]   L. Zhang, L. Harnefors, and H. P. Nee, "Power-synchronization control of grid-connected voltage-source converters," *IEEE Trans. Power Syst.*, vol. 25, no. 2, pp. 809–820, 2010.

[5]   E. Romero-Cadaval, B. Francois, M. Malinowski, and Q.-C. Zhong, "Grid-Connected Photovoltaic Plants: An Alternative Energy Source, Replacing Conventional Sources," *IEEE Ind. Electron. Mag.*, vol. 9, no. 1, pp. 18–32, 2015.

[6]   Z. Qing-Chang and G. Weiss, "Synchronverters: Inverters That Mimic Synchronous Generators," *IEEE Trans. Ind. Electron.*, vol. 58, no. 4, pp. 1259–1267, 2011.

[7]   L. Zhang and H. P. Nee, "Multivariable feedback design of VSC-HVDC connected to weak AC systems," *2009 IEEE Bucharest PowerTech Innov. Ideas Towar. Electr. Grid Futur.*, vol. 1, no. 1, pp. 1–8, 2009.

[8]   S. D'Arco, J. A. Suul, and O. B. Fosso, "Control system tuning and stability analysis of Virtual Synchronous Machines," *2013 IEEE Energy Convers. Congr. Expo. ECCE 2013*, pp. 2664–2671, 2013.

[9]   S. Golestan and J. M. Guerrero, "Conventional Synchronous Reference Frame Phase-Locked Loop is an Adaptive Complex Filter," *IEEE Trans. Ind. Electron.*, vol. 62, no. 3, pp. 1679–1682, Mar. 2015.

[10]   J. Alipoor, Y. Miura, and T. Ise, "Power system stabilization using virtual synchronous generator with alternating moment of inertia," *IEEE J. Emerg. Sel. Top. Power Electron.*, vol. 3, no. 2, pp. 451–458, 2015.

[11]   J. Rocabert, A. Luna, F. Blaabjerg, and P. Rodríguez, "Control of Power Converters in AC Microgrids," *IEEE Trans. Power Electron.*, vol. 27, no. 11, pp. 4734–4749, Nov. 2012.

[12]   C. N. Rowe and T. J. Summers, "Implementing the virtual output impedance concept in a three phase system utilising cascaded PI controllers in the dq rotating reference frame for microgrid inverter," in *2013 15th European Conference on Power Electronics and Applications (EPE)*, 2013, pp. 1–10.

[13]   E. Figueres, G. Garcera, J. Sandia, F. Gonzalez-Espin, and J. C. Rubio, "Sensitivity Study of the Dynamics of Three-Phase Photovoltaic Inverters With an LCL Grid Filter," *IEEE Trans. Ind. Electron.*, vol. 56, no. 3, pp. 706–717, Mar. 2009.

[14]   J. Dannehl, F. W. Fuchs, S. Hansen, and P. B. Thogersen, "Investigation of active damping approaches for PI-based current control of grid-connected pulse width modulation converters with LCL filters," *IEEE Trans. Ind. Appl.*, vol. 46, no. 4, pp. 1509–1517, Jul. 2010.

[15]   C. Lascu, L. Asiminoaei, I. Boldea, and F. Blaabjerg, "High Performance Current Controller for Selective Harmonic Compensation in Active Power Filters," *Power Electron. IEEE Trans.*, vol. 22, no. 5, pp. 1826–1835, 2007.

[16]   S. D'Arco and J. A. Suul, "A synchronization controller for grid reconnection of islanded virtual synchronous machines," in *2015 IEEE 6th International Symposium on Power Electronics for Distributed Generation Systems (PEDG)*, 2015, pp. 1–8.

[17]   W. Zhang, A. Luna, I. Candela, J. Rocabert, and P. Rodriguez, "An Active Power Synchronizing Controller for Grid- Connected Power Converters with Configurable Natural Droop Characteristics," in *2015 IEEE 6th International Symposium on Power Electronics for Distributed Generation Systems (PEDG)*, 2015, pp. 1–7.

[18]   J. Liu, Y. Miura, and T. Ise, "Comparison of Dynamic Characteristics Between Virtual Synchronous Generator and Droop Control in Inverter-Based Distributed Generators," *IEEE Trans. Power Electron.*, vol. 31, no. 5, pp. 3600–3611, 2016.

[19]   F. Gonzalez-Espin, V. Valdivia, D. Hogan, D. Diaz, and R. F. Foley, "Operating modes of a commercial and industrial building microgrid with electrical generation and storage," in *2014 IEEE 5th International Symposium on Power Electronics for Distributed Generation Systems (PEDG)*, 2014, pp. 1–5.

[20]   V. Valdivia, F. Gonzalez-Espin, D. Diaz, and R. Foley, "Low-frequency reduced-order modeling approach and implementation of grid emulation in hardware-in-the-loop platforms," in *2015 17th European Conference on Power Electronics and Applications (EPE'15 ECCE-Europe)*, 2015, pp. 1–7.